Decoupling of Closely Spaced Dipole Antennas for Ultrahigh Field MRI With Metasurfaces

Anna Hurshkainen, *Member, IEEE*, Masoud Sharifian Mazraeh Mollaei, Marc Dubois, Sergei Kurdjumov, Redha Abdeddaim, Stefan Enoch, Stanislav Glybovski, *Member, IEEE*, and Constantin Simovski

***Abstract*— Phased antenna arrays of dipoles are widely used in ultrahigh field (UHF) magnetic resonance imaging for creating the controllable radio frequency (RF) magnetic field distributions in a human body. Due to safety and imaging quality reasons each individual channel of the array should be decoupled—electromagnetically isolated from the others. The required number of channels is large and in some techniques the dipole antennas should be located in the close proximity of the human body. Their ultimately dense arrangement leads to a strong mutual coupling and makes the conventional decoupling structures inefficient. This coupling needs to be suppressed without a significant distortion of RF fields in the imaged area. In this work, we propose and study a novel decoupling technique for two UHF transceiver on-body dipole antennas. The decoupling is performed by a periodic structure of five parallel resonant wires referred to as a metasurface (MS). In contrast to conventional decoupling with a single resonant wire, the MS decoupled by means of excitation of a higher order coupled mode of the wires, which field is highly confined. The main advantage is a low distortion of the RF-field in the central region of the body.**

***Index Terms*— Decoupling, dipole antennas, metasurfaces (MSs), ultrahigh field (UHF) magnetic resonance imaging (MRI).**

I. Introduction

ULTRAHIGH FIELD (UHF) magnetic resonance imaging (MRI) operating with the static magnetic field strength over 7 T is an extensively developed tool for medical and research applications. UHF MRI requires additional efforts to overcome safety and imaging inhomogeneity issues [1]. As the wavelength inside the body tissues becomes comparable to a body size at the Larmor frequency of protons at 7 T, the wave propagation results in inhomogeneity of the magnetic radio frequency (RF) fields that causes such artifacts as dark voids on obtained body images [2]. To address this issue at UHF, phased arrays of individually driven antennas (loops or dipoles) surrounding a body are used for transmission of RF signals rather than single volume coils such as the birdcage coil [3]. Dipole antennas become nowadays more and more popular as elements of UHF body [4] and head [5] arrays due to a better compromise between SAR and transmit efficiency.

Typically coil arrays suffer from strong electromagnetic coupling between their elements: either reactive (capacitive or inductive, due to the fields created nearby the antennas) or resistive (due to excited conductivity currents in the body tissues). The mostly well-developed decoupling method for loop array elements is overlapping [6] which is however not applicable for dipole antennas. Apart from overlapping, a variety of decoupling methods for loop arrays have been proposed [7]–[11].

Regarding dipole UHF array elements, several decoupling approaches have been recently introduced. Namely, mushroom-type electromagnetic bandgap structures [12] and stacked resonators of magnetic type [13] grant the decoupling and weakly radiate into the body. Apart from the reduction of mutual coupling between antenna elements radiating at the same frequency, there is an important issue that occurs in multielement, multifrequency antenna systems. For instance, two neighboring antennas radiating at different (sometimes at close) frequencies behave as metal obstacles in the near field of each other. As a result, the radiation patterns and impedance frequency curves of both radiators are distorted. In [14], it was proposed to use electromagnetic cloaks shielding both antennas at frequencies outside of their own operational bands, that is at frequencies of neighboring antennas. With this mantle cloaking approach, several microwave metasurface (MS) designs have been proposed. There was a patterned metallic MSs consisting of vertical metallic strips printed on flexible dielectric substrates around two closely spaced dipoles [15], and a geometrically isotropic coupled dual-layer MS formed by subwavelength periodic I-shaped printed elements [16] both applicable at distances from 1/15 to 1/8 for the wavelength and, possibly, smaller. However, when s is as small as $\lambda/30$ (corresponds to a body array of 32 dipoles),

Manuscript received May 3, 2019; revised June 22, 2020; accepted July 4, 2020. Date of publication August 19, 2020; date of current version February 3, 2021. This work was supported in the theoretical part by the European Union's Horizon 2020 research and innovation program under grant agreement No 736937. The experimental part was supported by the Russian Science Foundation (Project 18-19-00482). *(Corresponding author: Anna Hurshkainen.)*

Anna Hurshkainen, Sergei Kurdjumov, and Stanislav Glybovski are with the Department of Physics and Engineering, ITMO University, 197101 Saint-Petersburg, Russia (e-mail: a.hurshkainen@metalab.ifmo.ru).

Masoud Sharifian Mazraeh Mollaei is with the Department of Electronics and Nanoengineering, Aalto University, 00076 Aalto, Finland (e-mail: masoud.2.sharifianmazraehmollaei@aalto.fi).

Marc Dubois is with Aix Marseille University, CNRS, Center for Magnetic Resonance in Biology and Medicine, 13005 Marseille, France, and also with Aix Marseille University, CNRS, Centrale Marseille, Institut Fresnel, 13013 Marseille, France (e-mail: marc.dubois@fresnel.fr).

Redha Abdeddaim and Stefan Enoch are with Aix Marseille University, CNRS, Centrale Marseille, Institut Fresnel, 13013 Marseille, France (e-mail: abdeddaim@fresnel.fr).

Constantin Simovski is with the Department of Electronics and Nanoengineering, Aalto University, 00076 Aalto, Finland, and also with the Department of Physics and Engineering, ITMO University, 197101 Saint-Petersburg, Russia.

Color versions of one or more of the figures in this article are available online at https://ieeexplore.ieee.org.

Digital Object Identifier 10.1109/TAP.2020.3016495

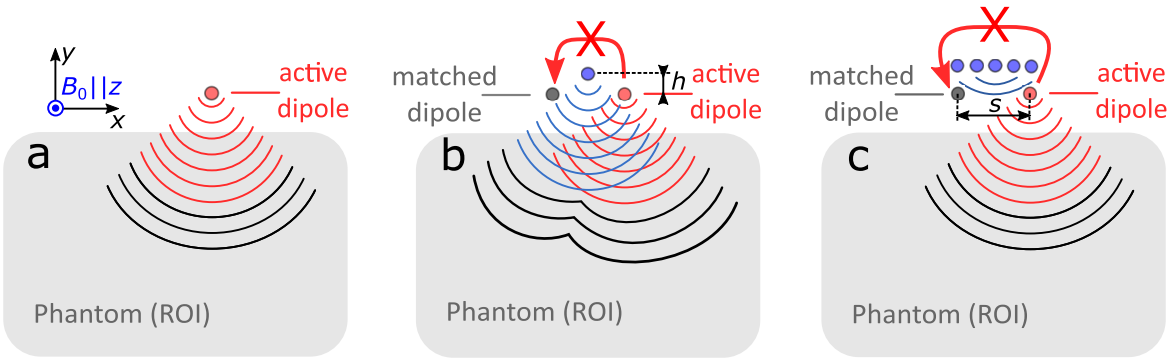

Fig. 1. Schematic of the proposed idea. (a) Active dipole (its cross section is shown as a red spot) creates a desired RF-field pattern in a phantom (the ROI). (b) Active dipole is isolated from another (matched) dipole by a single passive scatterer (resonant wire). The field scattered by the wire causes an RF-field interference destructive for imaging the ROI. (c) Decoupling is achieved by the excitation of a high-order mode in MS of multiple wires. Due to a strong confinement of field of the excited mode, MS creates only near fields and the desired field pattern created by the active dipole in the ROI is restored.

the above-referenced approaches are not applicable. In [17], the only suitable technique considering this geometrical constrain is shown. It is a properly loaded dipole scatterer (straight wire) centered in between the two dipoles. This passive decoupling method is proposed for two dipole antennas in free space.

In work [18], it was theoretically and experimentally shown that in the vicinity of the resonance of the unloaded wire scatterer, the latter grants a high though narrow-band isolation to the array of two dipoles separated by a gap as small as $s = \lambda/30$ and even smaller. The condition of the decoupling is the equivalent (nearly $\lambda/2$) length of the dipole antennas and the wire scatterer. In the presence of the equivalent of a human body, the similar technique had been previously demonstrated in [19] and claimed promising for 7-T MRI application. However, in [19], two monopole and not dipole antennas were decoupled and the gap s between them was much larger than $\lambda/30$. Moreover, in [18], we have shown that three parallel and coplanar dipole antennas are decoupled by two passive ones. In other words, in contrast with the claim of [17], this technique can be extended to $n > 2$. Next, in [20], we have reported this technique for the case when the human body phantom is present. The similar decoupling, as that obtained earlier for two dipoles in free space, was achieved by optimizing the position of the passive dipole. It was also shown that the decoupling is possible with a resonant scatterer different from the half-wavelength dipole.

The main drawback of the decoupling using a single resonant scatterer is a strong parasitic interference. Though the scatterer is passive, the dipole antenna located aside it at the distance $s/2 \approx \lambda/60$ induces a very high current in it. The radiation of the dipole array is engineered so that to maximize the magnetic (signal) field in the region of interest (ROI)—a part of the body to be imaged—and to minimize there the electric field causing the RF thermal noise and the patient body heating. Therefore, the reference pattern created by every dipole of the array should be maximally preserved when introducing a decoupling structure. This pattern is schematically shown in Fig. 1(a). The current induced in the decoupling scatterer sketched in Fig. 1(b) by the active dipole antenna has the opposite phase that is necessary to suppress the local electric field applied to the passive (matched) dipole antenna located at the distance s from the active one. As a result, the matched dipole can be isolated from the active one, but the scattered field of the induced current having the same or comparable penetration depth as that produced by the active dipole appears in the ROI as it is shown in Fig. 1(b). In [20], it was shown that this distortion is even stronger when the single decoupling scatterer has a different geometry—that of a split wire loop.

However, there is a strong demand of MRI-compatible decoupling techniques for ultimately dense dipole arrays that introduce minimal field distortion. Thus, the issue to be solved is the parasitic scattering accompanying the passive electromagnetic decoupling of dipoles. Here, it is worth to notice that known decoupling structures [12], [13] which grant a good compromise between the maximal isolation of two adjacent antennas and minimal distortion of the RF-field pattern in the ROI (compared to that created by a single scatterer) practically do not scatter. They are excited by the near field of the active dipole and create only the near fields themselves. However, they have a quite substantial width and demand the room $s \geq \lambda/10$ between two adjacent dipole antennas. This is why we need a new technical solution when the distance between the antennas is as small as $s \approx \lambda/30$.

Thus, the target of this work is to achieve the required level of isolation between two closely-spaced resonant dipole antennas (i.e., better than -10 dB when the antennas are matched) using a weakly scattering structure of width s no greater than $\lambda/30$ minimizing the field distortion in the ROI when compared to that corresponding to the single-scatterer decoupling technique. To possess low scattering, the structure must be weakly coupled to propagating plane waves, but strongly coupled via the near fields to the active and matched dipoles. This is possible if the structure supports high-order (not dipole-type) eigenmodes. We propose an appropriate structure made of five resonant thin wires referred to as an MS and use one of its high-order modes to decouple the dipole antennas minimizing the parasitic scattering by the decoupling structure.

In this article, we theoretically and experimentally answer the following questions.

1) Is it in principle possible to decouple ultimately coupled dipole antennas employing a high-order mode excited in the suggested decoupling structure?

2) Can a mode granting the decoupling in free space be used in the presence of the phantom—a homogeneous model of a human body? Which are peculiarities of the decoupling regime in the presence of the phantom?
3) How significant is the improvement of the RF magnetic field pattern inside the ROI in the MS decoupling case when compared to the case of the single decoupling scatterer?

II. Methods

A. Decoupling Structure

To meet the requirements for the decoupling structures for prospective on-body transceive dipole arrays, it was proposed to use a very dense planar array of half-wavelength wires [21]–[23] located over the gap s between the active and matched dipoles. The decoupling structure must be confined within the interdipole gap s. In this case, if the whole body coil contains multiple dipoles, each pair of neighboring dipoles could contain the same decoupling structure. In Fig. 1(c), the cross section of the suggested structure is schematically shown. We consider different numbers of wires N for the same width s, so the periodicity of the MS $a = s/(N-1)$ is parametrically swept but in all cases stays deeply subwavelength. Therefore, this array meets the general definition of the MS in accordance to [24]. The width of the MS is equal to the distance s between the dipoles, while the MS plane is raised at the height h above the plane of the antennas. MS wires have the same length $L = \lambda/2$ equal to the length of decoupled dipoles, where $\lambda \approx 1$ m is the wavelength in free space (the Larmour frequency 300 MHz corresponds to 7 T and the operational frequency should be sufficiently close to it).

B. Analytical Model

Our analytical model allows us to find the answer to the critical question 1 for the system of two closely spaced dipoles and to study the physics of decoupling with higher order modes in the proposed MS of straight resonant wires. It refers to the case when the phantom is absent and is based on the derivation of the impedance matrix Z_{ij} of the array of parallel wire dipoles (active, matched, and passive ones), where i and j stand for their indices. This matrix is obtained by the induced electromotive force method and connects the currents and voltages referred to the centers of every element of the dipole array. Our approach has been successfully validated for rather complex arrangements of finite-length metallic wires [25], [26]. The diagonal elements of the matrix are the self-impedances of the dipoles, and the off-diagonal elements are the mutual impedances. Since our array is fully composed by nearly half-wavelength thin-wire dipoles oriented along the same axis z, we can assume that in all wires the currents have a sinusoidal distribution

$$I(z) = I_0 \frac{\sin\left(k\left(\frac{L}{2} - |z|\right)\right)}{\sin\left(k\frac{L}{2}\right)} \tag{1}$$

where I_0 is the current phase in the middle of the wire.

With this approximation, we can calculate the self- and mutual impedances of an arbitrary system of dipoles using a standard derivation based on formula

$$Z_{ij} = -\frac{1}{I_{0i} I_{0j}} \int_{-\frac{L}{2}}^{\frac{L}{2}} E_{ij}(z) I_i(z) dz \tag{2}$$

where E_{ij} is the z-component of the electric field produced by dipole j at the point with the coordinate z on the axis of ith dipole and L is the dipoles' length. Equation (2) expresses the induced electromotive force method for straight wires.

Analytical expressions of dipole near fields can be found in [25]. Self-impedances are computed with the same equation (2) by evaluating the electric field at a distance equal to the round wire radius. The impedance matrix, and then the S-matrix assuming the port characteristic impedance Z_0, is calculated for a range of frequencies around the proton Larmor frequency of 7-T MRI (300 MHz). The validity of our implementation of the impedance matrix method is discussed in further details in the Appendix.

This approach was applied to the system of two dipole antennas in the absence and in the presence of a decoupling scatterer according to the conventional approach [17], where the scatterer is a wire of the same length as the dipoles, but loaded at the center by a lumped element. Also, it was applied to the system of two and more half-wavelength dipole antennas in the absence and in the presence of one or more decoupling scatterers representing the unloaded (shortcut) wires of the same length [18]. Here, we apply this approach to the dense planar array of half-wavelength wires comprising the decoupling MS. In the expressions, we labeled two decoupled dipole antennas with indices 1 and 2, while the rest of indices corresponds to the $N = n - 2$ passive wires of the MS. Although the calculated Z- and S-matrices (both $n \times n$) contain relevant information, the coupling coefficients S_{12} obtained using this method in a standard way [25] imply that the passive scatterers are loaded with the impedance $Z_0 = 50\ \Omega$—that of the wave port connected to the dipole antennas. To account for the fact that our MS is composed of *short-circuited* wire scatterers, we apply the method originally described in [27]. It allows us to reduce the n-port S-matrix to a 2×2 matrix between the two dipoles taking into account the short-circuiting load reflections from the passive scatterers. We defined Γ_L a diagonal matrix of size $n-2$ containing the load reflection coefficients from the scatterers. For short-circuited wires, this coefficient is equal to -1 leading to $\Gamma_L = -I_{n-2}$. The reduced S-matrix denoted as S^{r} reads

$$S^{\mathrm{r}} = P_{11} + (P_{12}\Gamma_L)(I - P_{22}\Gamma_L)^{-1} P_{21}. \tag{3}$$

Here P_{ij} are the submatrices defined as follows:

$$S = \left(\begin{array}{c:c} P_{11} & P_{12} \\ \hdashline [2pt/2pt] P_{21} & P_{22} \end{array}\right) = \left(\begin{array}{c:ccc} S_{11} & S_{12} & \cdots & S_{1n} \\ \hdashline S_{21} & S_{22} & \cdots & S_{2n} \\ \hdashline [2pt/2pt] \vdots & \vdots & \ddots & \vdots \\ S_{n1} & S_{n2} & \cdots & S_{nn} \end{array}\right). \tag{4}$$

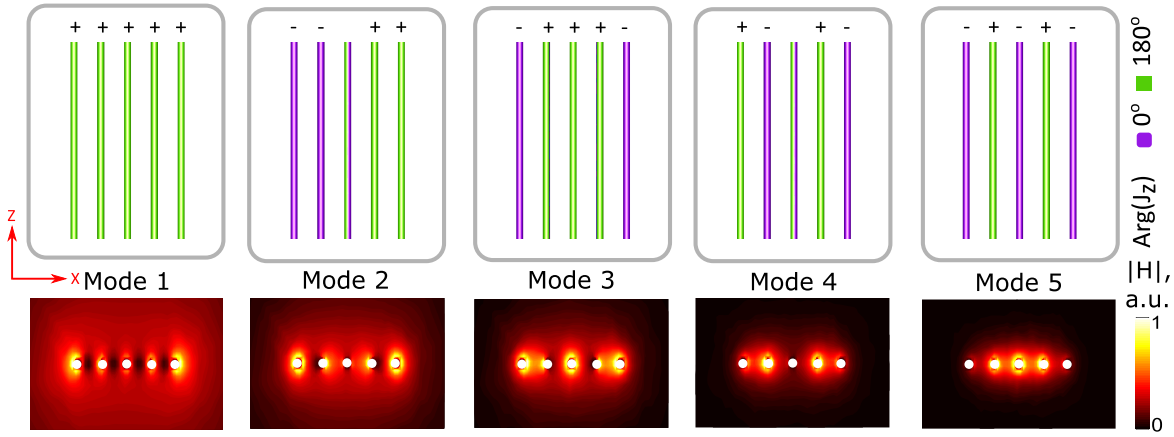

Fig. 2. Eigenmodes of MS composed of $N = 5$ half-wave wires. Top row: phases of wire currents. Bottom row: transverse-plane magnetic field magnitude patterns.

The off-diagonal elements of the reduced S-matrix ($S_{12}^{\mathrm{r}} = S_{21}^{\mathrm{r}}$) give us the coupling of mismatched dipoles in the presence of the MS. In the MRI applications, these dipoles should be matched to Z_0. Therefore, to determine the true isolation between the dipoles, we should assume an ideal matching of both dipoles at each frequency of our interest. The coupling coefficient S_{12}^{*} defined as the transmission coefficient of a two-port system matched from both sides can be found as the function of frequency in the resonance band of the dipoles from S_{12}^{r}. We have done this recalculation using the method described in [28].

C. Full-Wave Simulations

Full-wave simulations were performed using the commercial software CST Microwave Studio. In the absence of the body phantom, these simulations allowed us to find the eigenmodes of the MS and to identify these modes excited by the active dipole in the presence of the matched dipole to be isolated. To solve the eigenmode problem, the eigenmode solver of was used. The wires' current phases of the proposed MS composed of $N = 5$ half-wave wires and respective near magnetic field distributions corresponding to five different eigenmodes were calculated. The obtained results are illustrated in Fig. 2.

In the presence of the phantom—a homogeneous volume with the averaged material properties of human body tissues—full-wave simulations were used to calculate the S-parameters of two dipoles and to refer the decoupling regimes to the explicit eigenmodes of our MS. With this purpose, we analyzed the currents induced in its constitutive wires and magnetic field patterns created by that currents in their vicinity.

In our numerical simulations, we considered two half-wave dipoles with two 50 ω lumped ports and the MS of N half-wave wire scatterers. The number of wires was parametrically changed between 2 and 6 for different heights h over the plane of two dipoles. Though it was shown that one of the high-order modes can be used for decoupling with low field distortion for any $N \geq 3$, the case with $N = 5$ was investigated in more detail. It was done to analyze the possible conditions for this decoupling and other available decoupling regimes. $N = 5$ was chosen as a compromise based on the following considerations. We expect that one of the high-order modes of the MS can grant decoupling while not distorting the field in the phantom. In contrast to the single scatterer decoupling technique, we expect that the MS should realize a nonradiative distribution of effective surface current with many spatial phase oscillations in x-direction. The higher is the order of the excited mode in the MS, the weaker is the expected field distortion in the phantom. Therefore, it is beneficial to use MSs with larger N to be able to excite modes of as high order as possible. At the same time, in practice, the wire diameter is limited and cannot be arbitrary small. As a result, the multimode excitation of the proposed MS becomes impossible when the interwire distance $s/(N-1)$ becomes comparable to two wire diameters due to high interwire capacitance. It can be shown that as thick circular wires wide conducting strips are used to build the MS, the gap capacitance between the conductors disable high-order modes. In this limiting case, the whole structure supports only a single dipole mode effectively turns into a single scatterer. On the contrary, if a wire thickness stays small in comparison to the wire period, the wires could of arbitrary cross section shape. We considered round wires for simplicity. In other cases, an effective radius of a circular wire can be used to calculate the corresponding self-impedances.

The active and matched dipoles [see Fig. 1(b) and (c)] in these situations were thin wires with the given radius $r_0 = 1$ mm and the length $L = 500$ mm to be resonant around the Larmour frequency 300 MHz. The phantom had the dimensions $600 \times 400 \times 400$ mm^3 and the material properties: $\epsilon_r = 80$, $\sigma = 0.5$ S/m corresponding to saline water. The distance s between the two dipoles was 30 mm, which is around $\lambda/30$. Since the width of the MS was equal to s, for $N = 5$ wires, the interelement spacing was 7.5 mm, and the height h of the MS over the plane of the dipoles h was varied from 10 to 35 mm. Simulations were performed using integral equation solver. S-parameters of the active dipoles and magnetic field distribution inside the phantom were calculated. The actual isolation $|S_{12}|^{*}$ when both dipoles are matched to $Z_0 = 50$ ω at all frequencies was calculated as proposed in [28].

D. Measurements

To confirm the theoretical and numerical results, we measured S-parameters of the two-dipole array and magnetic field patterns in a homogeneous liquid phantom (0.9% NaCl water solution) of the same sizes as in simulations. Two dipoles were implemented as wire strips of the width 4 mm on 0.5 mm thick FR4 substrates, and the MS contained five round wires of brass with the length 500 mm and the radius $r_0 = 1$ mm on a foam holder. In S-parameter measurements, the dipoles were connected to a vector network analyzer (VNA) using two symmetric transmission lines–each one composed of a pair of 50 ω coaxial cables driven in the differential mode to avoid the cable effect.

The main (horizontal) component of the magnetic field created in the phantom by the active dipole was measured using a 3-D near-field scanner with a small loop probe, while the matched dipole was loaded by 50 ω at the center. Measurements were done by moving the probe immersed in the liquid of the phantom.

It is worth noting that we have made all measurements using typical powers available with VNAs (mW levels). Real transmit coils for body imaging at 7 T should be designed to operate under powers up to 2 kW per channel in pulse. We did not perform direct measurements at such high power levels but verified the most important safety aspect for future experimental characterization of the proposed MS in MRI on a phantom. In particular, we checked the peak local value of E-field nearby conductors of the MS in simulation and ensured it was one order of magnitude lower than the electric breakdown threshold. Characterization of SAR for the safety of volunteers using detailed body models is a part of future work.

III. Decoupling by the MS

A. MS Decoupling in Free Space and Relation to Eigenmodes

Five wires of our MS are electromagnetically coupled very strongly because the MS period is as small as $s/4 \approx \lambda/120$. As a result, the MS supports $N = 5$ hybridized eigenmodes [29]. All eigenfrequencies are located near the resonance frequency of an isolated wire scatterer but clearly distinguished on the frequency axis. These modes have very different magnetic field patterns which allow us to easily classify them. The multipolar nature of these modes is clear from Fig. 2 which depicts by the colors the phases of the currents in the wires at all five eigenfrequencies and the corresponding magnetic field patterns (distributions of the magnitude) in the central transverse plane.

Due to all wire currents flowing in phase, it is evident that mode 1 is the electric dipole mode. As we expect, in terms of decoupling, this mode behaves similar to a resonant mode of a single scatterer. The mode 2 is antisymmetric in terms of the current distribution. It is the combination of an off-diagonal (zx-component) electric quadrupole and a magnetic dipole oriented along y. The values of the quadrupole and magnetic dipole moments in this mode are balanced that makes the electric quadrupole (off-diagonal) and magnetic dipole not distinguishable in what concerns their electromagnetic fields the central transverse plane (H-plane of the array) [30]. Therefore, the currents of this mode create in the transverse plane the near magnetic field identical to that of a horizontal loop of the same length [31], [32]. This field is presented in Fig. 2 (bottom). The higher modes (3–5) are characterized by faster spatial oscillations of the effective surface current across the MS, visible in Fig. 2. Mode 3 is the balanced combination of an off-diagonal magnetic quadrupole and an electric dipole, modes 4 and 5 are balanced combinations of the aforementioned multipole moments and higher order electric and magnetic multipoles.

As we expected, when the mode order increases the corresponding electromagnetic field better concentrates around the MS. It becomes weakly coupled to plane waves and its radiation decreases. Despite the radiation of the high-order mode is low, their near fields at the distance comparable to one period a from the wires is high. It means that depending on the height h of the MS one of the high-order modes can couple to both active and matched dipoles through near field. At the same time, once excited, this mode would not create the undesirable interference in the subject. Therefore, the mode fields presented in Fig. 2 already illustrate the proposed concept.

Let us now consider two dipoles separated by the distance $s = \lambda/30$ in the presence of the 5-wires MS with the width s, located at the height h over the dipoles.

To study the possibility of decoupling due to excitation of different eigenmodes of the considered MS, we have analytically calculated the mismatched S_{12} coefficient, the true isolation coefficient S_{12}^* (corresponding to the case when both dipoles are impedance matched to 50 ω), and the magnetic fields created when the active dipole is fed in the frequency range 285–305 MHz for MS heights h ranging from 0 to 40 mm.

For comparison, we consider the decoupling granted by a single resonant wire scatterer [18]. It can be shown that it affects S_{12} of the two dipoles only around one frequency, that is the frequency of its resonance at 298.9 MHz [case 1 in the first plot in Fig. 3(a)]. At the same frequency, it provides $|S_{12}|^* = -32$ dB at the optimal height $h = 9.5$ mm as shown by the dashed curve in the second plot in Fig. 3(b). The corresponding field pattern (case 1) is shown in Fig. 3(b). It can be seen that the passive scatter produces an equally strong field as the active dipole. But since it is excited out-of-phase and cancels the induced current in the matched dipole, it causes destructive interference in the direction downward. This is the reason for inhomogeneity in MRI when the same approach distorts the magnetic field in a phantom.

In the following, we will study all decoupling regimes providing by our MS one by one and explain them in terms of the excited eigenmodes. This discussion will identify at which frequencies high-order mode lead to decoupling and observe other existing regimes. The results of parametric variation of h are shown for S_{12}^* in Fig. 3(d). From this plot, it is clearly seen that there are two areas, where isolation is provided, that is $|S_{12}|^* < -10$ dB: the broadband region for h from 25 to 35 mm and the narrow band region for h from 6 to 13 mm. To understand these decoupling mechanisms, let us discuss the frequency behavior of S-parameters

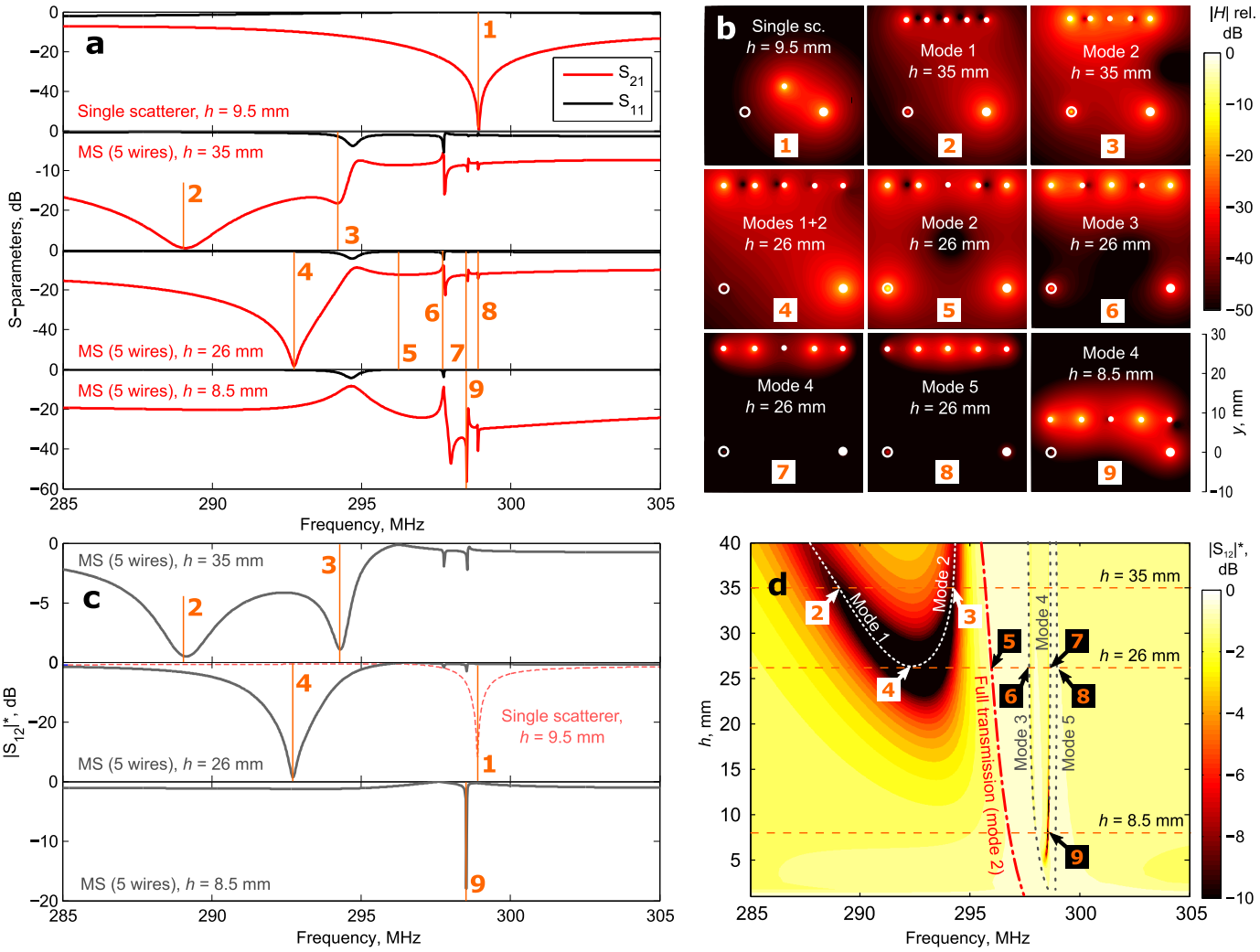

Fig. 3. Results of analytical calculations of the isolation levels and fields provided by the MS of $N = 5$ wires in free space and their comparison with the case of a single wire scatterer. (a) Coupling coefficient in the mismatched regime $|S_{12}|$ versus frequency. Nine characteristic decoupling regimes are numbered. (b) Magnetic field patterns of the active dipole in the presence of the decoupling MS in these regimes (nine panels correspond to nine regimes). (c) Actual isolation of two matched dipoles is seen in the plots of $|S_{12}|^*$ versus frequency. (d) Dependence of $|S_{12}|^*$ on both height h of our MS and frequency.

and related magnetic field patterns. Any excitation source coupled to the MS generally excites a linear combination of modes depicted in Fig. 2. Once, the mode fields are known, the complex coefficients of this linear combination at an arbitrary frequency can be calculated numerically using expansion into eigenmodes. However, our goal was limited to identification of the mode, which is mostly responsible for strong isolation in different regions of Fig. 3(d) without quantitative determinations of specific eigenmode contribution to the dipole field inside a phantom. It is well known that in the case of a high-quality factor (narrowband resonance) and in the absence of mode degeneration, the contribution of a mode around its resonance frequency is dominant. This fact allowed us to identify modes by comparing the pattern of the field excited by the dipole in the MS in any regime of interest, to eigenmode fields presented in Fig. 2. In fact, the excitation of all the modes of the MS can be observed in the frequency dependence of the mismatched S-parameter S_{12}. Such curves are shown in the second, third, and fourth plots of Fig. 3(a) for $h = 35$, 26, and 8.5 mm correspondingly.

When the height of the MS is as large as 35 mm, one observes two relatively shallow minimum of $|S_{12}|$ at 287 and 294 MHz [panels 2 and 3 in in Fig. 3(b)]. One can check that the true isolation level reaches -10 dB at both these frequencies. Looking for the field pattern in panel 2 and comparing to Fig. 2, one can conclude that the first minimum is achieved due to excitation of the dipole mode of the MS. Since the MS has multiple wire currents instead of one, this regime corresponds to higher h than in case 1 (single scatterer). This case 2 is not the regime we are looking for, because it is similar to decoupling using just one scatter. All the currents in the MS wires are induced in phase, but with the opposite phase to the active dipole. However, this side result can be a useful modification of the single-wire approach as explained below. In the second, minimum decoupling is provided by the excitation of mode 2, which is evident from the corresponding field pattern [see panel 3 in Fig. 3(b)].

As h reduces, the two shallow minimum of $|S_{12}|^*$ merge into one at 292.6 MHz as can be seen in Fig. 3(d). The cut of this diagram at $h = 26$ mm is shown in the second plot of Fig. 3(c),

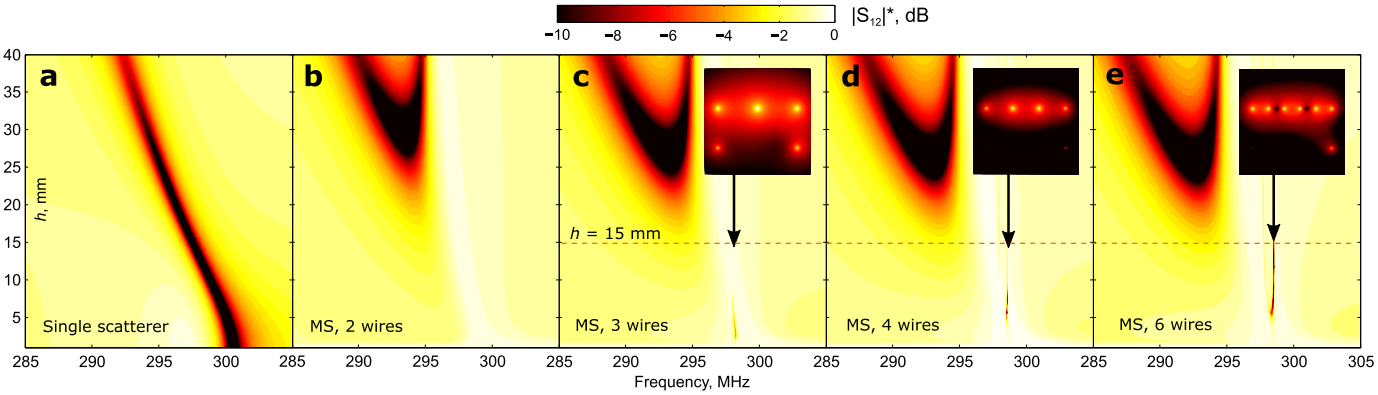

Fig. 4. Results of parametric variation of the inter-wire spacing by changing the number of wires. Analytically calculated $|S_{12}|^*$ versus the height h and frequency for (a) single scatterer and (b)–(e) decoupling MSs with $N = 2, 3, 4, 6$.

where the best isolation of −55 dB is reached. At this height, there is only one relatively broad decoupling band, which is much broader than one provided by a single scatterer (compare to the dashed curve on the same plot). The decoupling band measured at the level $|S_{12}|^* = -10$ dB is 4.7 times broader with the MS of five wires than with the single scatterer (2.8 MHz instead of 0.6 MHz). This broadband decoupling can be explained by degeneration of modes 1 and 2, which can be observed in case 4 marked in Fig. 3(c), where the field in the vicinity of the MS is a superposition of the symmetric mode 1 and antisymmetric mode 2. Moreover, it is worth noting that at any h there is a frequency where instead of decoupling the MS leads to almost full transmission between the dipoles ($|S_{12}|^*$ is close to 0 dB). This regime is shown by a red dashed-dotted curve in Fig. 3(d). The example of this regime for $h = 26$ mm is case 5. From Fig. 3(b), one can deduce that this transmission is also provided by the resonant excitation of mode 2.

Therefore, our analysis based on Fig. 3(b) shows that at heights $h \geq 25$ mm decoupling in the proposed MS is achieved due to modes 1 and 2 (cases 2 and 3), or their combination in the particular case (case 4). Since the field of these modes is not confined compared to the field of a single scatter, neither mode 1 nor 2 can solve the problem of field distortion in the phantom. So, let us now investigate the effect of high-order modes (with the order of 3 and larger).

Excitation of the high-order modes 3–5 affects $|S_{12}|$ at any h if only the frequency is close to the corresponding resonances. Thus in the third plot of Fig. 3(a), cases 6–8 correspond to these higher order modes. Despite at $h = 26$ mm, they do not isolate efficiently ($|S_{12}|^* \approx -2$ dB), the corresponding modes are clearly excited. One can recognize their field patterns by comparing the plots in panels 6–8 of Fig. 3(b) with the mode fields depicted in Fig. 2. Inspecting the diagram of Fig. 3(d) one can conclude that an efficient isolation is possible only at the resonance of mode 4 for the heights between 6 and 13 mm. The optimal height for this mode is $h = 8.5$ where $|S_{12}|^*$ of −16 dB is achieved. Here the −10 dB bandwidth of decoupling is only 40 kHz. In this regime, the field pattern corresponds to case 9 in Fig. 3(d).

Therefore, we can made the next conclusion. Despite all high-order modes 3–5 can be excited at their resonant frequencies, only mode 4 leads to decoupling of two dipoles. This fact can be explained by achieving at $h = 8.5$ mm, the optimal coupling coefficient between this mode and the dipoles, which is impossible for modes 3 and 5. Therefore, mode 4 does provide the desired high-order mode decoupling regime (case 9), which is the main result of this article.

Next, we parametrically studied the role of separation between the MS' wires. Since, by design, the full width of the MS should be equal to the separation between the active and matched dipole s, we varied N. In Fig. 4, we compare the behavior of $|S_{12}|^*$ depending on frequency and height h for N=1,2,3,4, and 6. For the single scatterer considered for comparison in Fig. 4(a), one observes only one resonance that grants decoupling for a very broad range of h. When $N = 2$ (a simplest MS) mode 2 appears. The more wires in the MS, the more eigenmodes are excited. It means that for different $N \geq 2$ a broadband regime of decoupling is available, with the decoupling bandwidth increasing with N, but it can be shown that in terms of field distortion it is similar to the effect of a single scatterer. As to our expected regime, Fig. 4 shows that for any $N \geq 3$ there is one narrow-band regime related to one of the higher order modes which provides isolation. The optimal height increases with N, while the frequency is almost the same. Now let us highlight the systematic approach to finding the proper high-order decoupling regime. It was shown that for $N = 4, 5$ and 6 the high-order decoupling regime is always due to mode with the fourth order. For $N \geq 4$ this mode is antisymmetric like mode 2, but has a more confined field. One can use a wire MS as a separate multimode resonator for decoupling only if h is greater than a MS period. In this case, decoupling is possible to achieve with modes of even orders. While mode 2 is too radiative, mode 4 for $s = \lambda/30$ is optimal in terms of it field confinement and its excitation magnitude. To use this mode, h should be in the range from 1.5 to 2 periods of the MS. Mode 6 for $N \geq 6$ is the next even mode, so it could be also used for decoupling. However, in our problem, it does not provide decoupling due to an insufficient coupling to the dipoles at any heights larger than the MS period. It should be noted that at h smaller than the period the dipoles and the MS wires form a common structure of $N + 2$ coupled resonators and no systematic approach based on MS modes can be proposed.

Investigation of near-field interactions between the dipoles and wire MSs allows us to distinguish two regimes.

1) *Low-Order Mode Regime:* It is achievable with any MS with $N \geq 2$ and provides broader band of decoupling than a single wire scatterer. However, similar to a single scatterer it causes field distortion in the direction downward;
2) *High-Order Mode Regime:* It is achievable with any MS with $N \geq 3$ and provides narrowband decoupling due to excitation of a high-order mode (with orders larger or equal to 3) having strong confinement of their fields and low radiation downward. This mode has the main interest and it will be investigated in the presence of a phantom numerically and experimentally in the following sections.

B. MS Decoupling in the Presence of the Phantom

In the presence of the phantom, our analytical model is not applicable, and for this case full-wave numerical simulations were performed. The phantom was located 20 mm below the plane of the dipoles. Henceforth, we consider the MS composed of $N = 5$ wires with the separation of 7.5 mm. All other parameters are the same as in the previous subsection. The same parametric variation of the MS height h was repeated numerically to find the optimal height providing the best isolation. The results confirm that in the presence of the phantom the same two decoupling regimes are available: a relatively broadband low-order mode regime of decoupling due to the excitation of modes 1 and 2 at the same frequency and a relatively narrowband high-order regime of decoupling due to mode 4. The said is confirmed by $|S_{12}|^*$ versus frequency plots calculated for two corresponding optimal heights $h = 30$ and 10 mm, shown together with the results for the absence of decoupling and the single decoupling scatterer cases in Fig. 5. The insets in the plot represent the magnetic field patterns created by the active dipole in the vicinity of the MS near the corresponding resonance frequencies (cases 4 and 9 in Fig. 5).

Comparing to cases 4 and 9 in Fig. 3(b) one can see that excitation of the same modes is responsible for decoupling in the presence of the phantom: the combination of modes 1 and 2 at $h = 30$ mm (case 4) and mode 4 at $h = 10$ mm (case 9). Thus, in the presence of the phantom, the MS provides the same low- and high-order decoupling regimes, where the latter is, again, due to excitation of mode 4. Therefore, this desirable regime is stable with respect to a phantom. Meanwhile, the optimal frequencies and heights obtained analytically in free space and numerically with a phantom are slightly different. With the phantom the combination of modes 1 and 2 provides $|S_{12}|^* = -28$ dB at 297.7 MHz, while mode 4 reaches the isolation of -18.6 dB at 282.6 MHz. This means -23 and -13.6 dB improvement correspondingly over the case with no decoupling.

Comparing decoupling bands, the simulation confirms that the MS operating due to the combination of modes 1 and 2 provides a wider band than the single scatterer. The band in which the improvement of isolation is at least -10 dB is 6.6 MHz with the MS at $h = 30$ mm instead of 3 MHz with

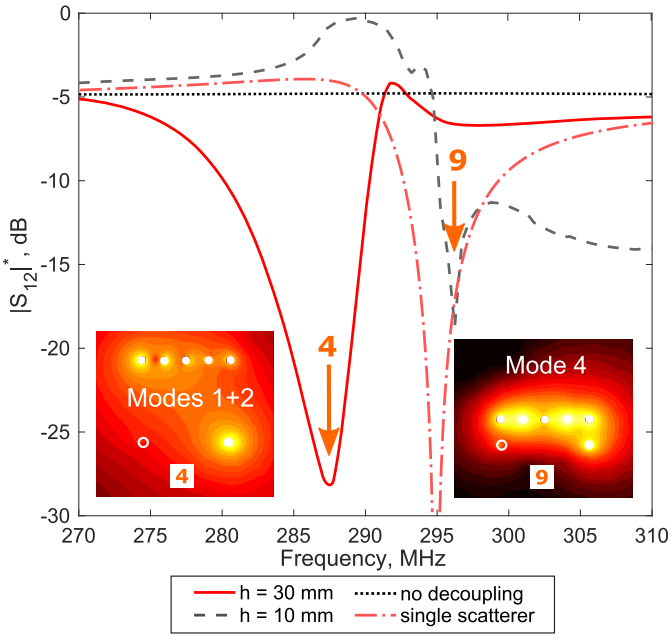

Fig. 5. Numerically calculated $|S_{12}|^*$ of two dipoles in the presence of phantom without decoupling, with single scatterer and with MS at $h = 30$ and 10 mm. Insets: normalized magnetic field patterns created by active dipole in corresponding cases indicated by numbers similar to Fig. 3(b).

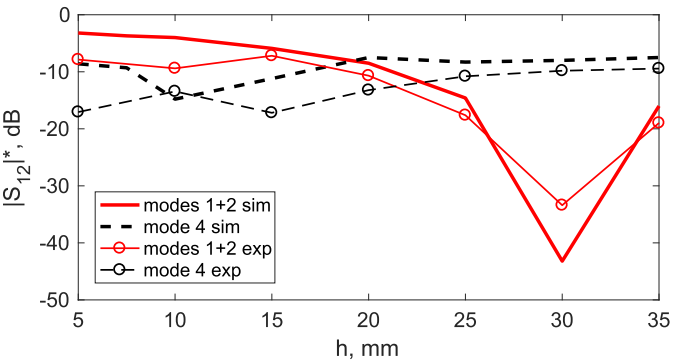

Fig. 6. Numerically calculated and measured $|S_{12}|^*$ versus height h of two dipoles in the presence of phantom at resonant frequencies corresponding to: combination of modes 1,2 (297.7 MHz) and mode 4 (282.6 MHz).

the single scatterer. This is an improvement of the conventional approach with one wire scatterer, however, as shown below, this regime still leads to field distortion in the phantom and therefore, does not solve our problem. Mode 4 provides the same isolation improvement in the band of only 0.7 MHz. It is noted that in the presence of the phantom which brings electromagnetic losses into the whole system the bands of the eigenmodes and, respectively, the decoupling bands are wider in comparison to their values in the free-space case.

To demonstrate the sensitivity of low- and high-order mode decoupling regimes of the MS to variation of h, the corresponding dependencies of $|S_{12}|^*$ have been calculated. The results are shown in Fig. 6 using lines with no markers.

Now let us compare the effect of each of the considered decoupling regimes on the magnitude distribution of magnetic field created by the active dipole in the phantom.

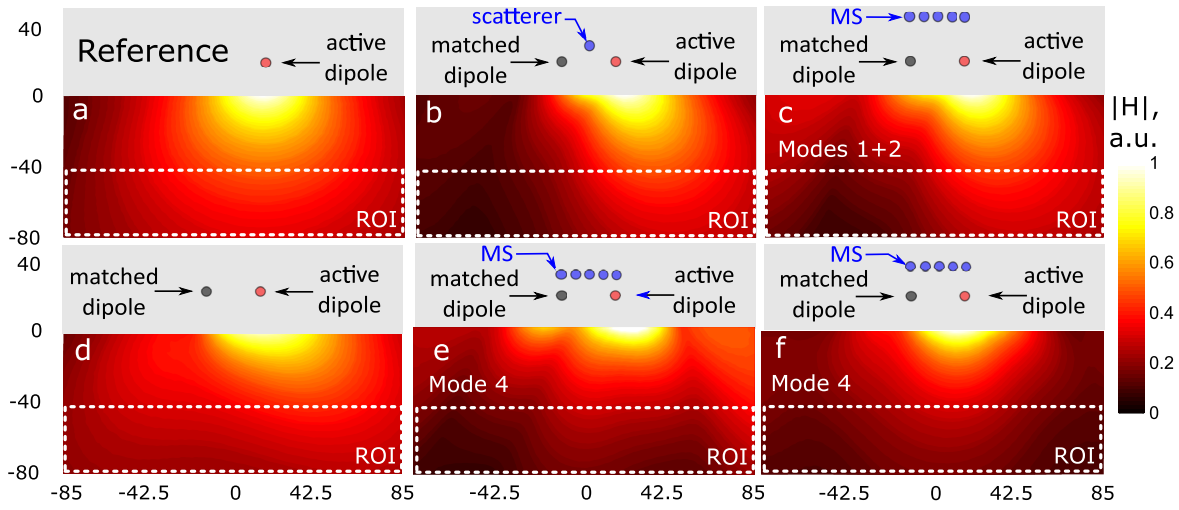

Fig. 7. Simulated magnetic field patterns normalized by maximum in the central axial slice of the phantom. (a) Reference case of one dipole. (b) Active dipole and matched dipole decoupled by a passive scatterer. (c) Same but decoupled by MS with modes 1+2 ($h = 30$ mm). (d) Same but decoupled by MS with mode 4 ($h = 10$ mm). (e) Same but decoupled by MS with mode 4 ($h = 15$ mm).

The normalized numerically calculated patterns are presented in Fig. 7. While the depth of the phantom in the simulations was 400 mm, the ROI was chosen to be the layer at the depths from 40 to 80 mm from the phantom surface. In the body imaging application at 7 T, it corresponds to the depth of internal organs such as the prostate. The ROI is indicated in Fig. 7 by a dashed-line contour. The reference case is shown in Fig. 7(a), where a single active dipole at the height 20 mm over the phantom creates in the ROI a relatively homogeneous field. The aim of our decoupling method is to provide a similar pattern in the presence of a matched dipole while keeping high isolation between the dipoles ($|S_{12}|^* < -10$ dB). In the presence of the second (matched dipole) at the distance $s = \lambda/30$, the field distribution does not degrade in terms of homogeneity as shown in Fig. 7(d). However, the magnitude $|H|$ in the middle of ROI normalized by the square root of the accepted power reduces by 40%. In addition to a poor isolation with $|S_{12}|^* = -5\ dB$, this is a reason why a decoupling structure is required. It is noted that in Fig. 7 all the patterns are normalized by the maximum value to compare the homogeneity.

When the same dipoles are decoupled by a single scatterer at its optimal height the isolation reaches -30 dB, but there is a strong distortion of the signal (magnetic) field in the ROI due to the destructive interference discussed above. The interference minimum occupies the left part of the ROI and is clearly seen in Fig. 7(b). To quantitatively analyze the field distortion, we have calculated the additional comparative scatter plot corresponding to the single-scatterer decoupling and the reference case. This plot is shown in Fig. 8(a). The plot demonstrates pixel-by-pixel comparison between the magnetic field in the reference case and one in the presence of the decoupling element. The data used correspond to the ROI indicated in the simulated patterns of Fig. 7. It is noted that both field patterns to be compared pixel-by-pixel are normalized for the maximum value in the ROI; therefore, both the horizontal and vertical axes in the scatter plot have the maximum value of 1. When all points of the scatter plot are at the diagonal red line, the decoupling element is ideal and does not distort the shape of the field distribution of the active dipole. Due to normalization, the absolute values of the created fields in the ROI do not affect the shape of the cloud of points. The closer the cloud of points to the red line, the better in terms of the field-shape distortion. As seen from Fig. 8(a), distortion due to the single decoupling scatterer in the phantom is strong.

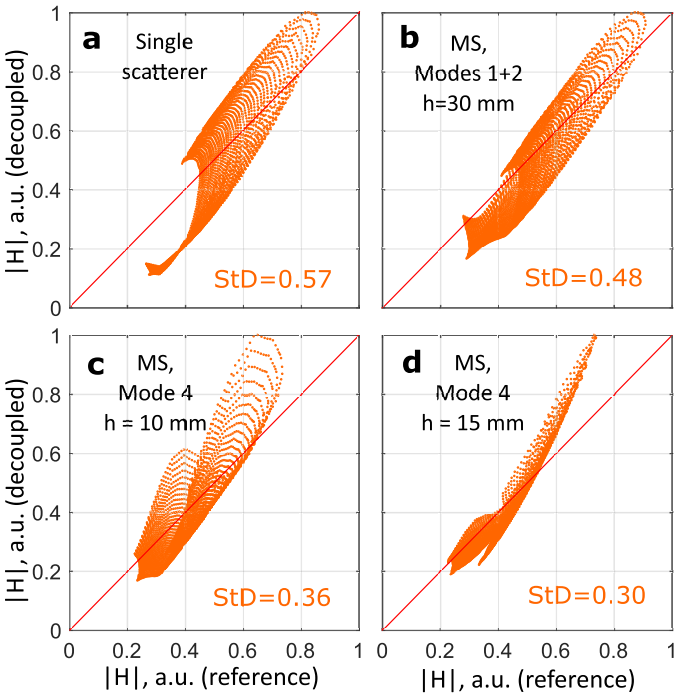

Fig. 8. Pixel-by-pixel comparison of numerically calculated normalized H-field magnitude in the case with decoupling (vertical axis) versus H-field magnitude in the reference case (horizontal axis) in the transverse plane of the phantom. (a) Single scatterer. (b) MS, modes 1+2 at $h = 30$ mm. (c) MS, mode 4 at $h = 10$ mm. (d) MS, mode 4 at $h = 15$ mm.

We calculated the ratio of the normalized H-field magnitudes in the decoupled and reference cases, and found its standard deviation (StD) around the mean value of 1.0. Calculated in such a way StD is smaller for the cloud of points which is more compact around the diagonal line in Fig. 8. In the case of the single-scatterer decoupling StD equals 0.57.

Next let us consider the case of the MS operating in the combination of modes 1 and 2. Due to the contribution of the two modes at the same frequency, in this regime, we have more broadband decoupling with the best isolation level of −28 dB. The dipole mode 1 creates scattering similarly as the single scatterer. Indeed, in this low-order mode of the MS, it is seen in Fig. 7(c), that similar to a single scatterer a low-field region (local minimum) appears due to the destructive interference in the left part of the ROI. However, this destructive effect is not as strong as for the single scatterer thanks to the presence of mode 2 having a more confined field than mode 1. Indeed, in Fig. 7(c), the field in the minimum is higher than in the corresponding point in Fig. 7(b). Despite decoupling using the combination of modes 1 and 2 of the MS is better than with a single scatterer in terms of a bandwidth of decoupling, the field distortion in the phantom is not much weaker. The said is confirmed by comparison of Fig. 8(a) and (b), where the cloud of points at a scatter plot for the low-order MS regime is more compact and the standard deviation reduces from 0.57 to only 0.48.

Now let us consider the field effect in the phantom in the most attractive regime of decoupling, the high-order mode regime based on excitation of mode 4. For the optimal height $h = 10$ mm, the normalized magnetic field in the phantom corresponding to case 9 with the isolation of −18.6 dB at 282.6 MHz indicated in Fig. 5 is shown in Fig. 7(e). It can be seen that the field in the ROI becomes more homogeneous—the interference minimum spreads. The field becomes closer to the active dipole field, as can be checked looking at the plot in Fig. 8(c), and the standard deviation further reduces to 0.36. Therefore, using mode 4, one can reduce the destructive interference in the phantom keeping the isolation improvement by around 13 dB in comparison to the reference case without any decoupling structure.

Moreover, from Fig. 6, it is seen that if h changes from 10 to 15 mm, the isolation still holds at the target level of −10 dB. At the same time, one can ensure that for this elevated position of the MS operating at the resonance of mode 4, one can even better reproduce the desirable reference field pattern in the phantom. Indeed, as shown in Figs. 7(f) and 8(d), the field shape becomes much closer to one of the active dipole alone. The standard deviation in this case reduces to 0.3, which is almost two times smaller than for the conventional decoupling technique with the single resonant scatterer. Therefore, the high-order mode decoupling can be used in two variations. For the first one, at $h = 10$ mm the best isolation improvement is achieved (at the operation frequency the coupling coefficient decreases by 13 dB) with noticeably lower field distortion in the ROI as compared to the case of the single decoupling scatterer. However, the parasitic interference is still visible in the top part of the phantom. In the second variation $h = 15$ mm and the isolation keeps on the target level of −10 dB (only by 5 dB better than with no decoupling). However, in this regime, the MS creates practically no destructive interference in the whole phantom. This result answers to both questions 2 and 3 formulated in the Introduction. Below we confirm our theoretical findings experimentally.

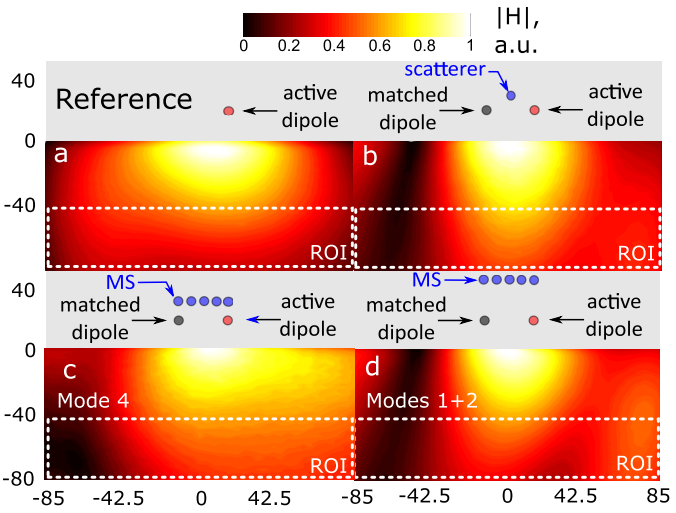

Fig. 9. Measured magnetic field patterns normalized by maximum in the central axial slice of the phantom. (a) Reference case of one dipole. (b) Active dipole and matched dipole decoupled by a passive scatterer. (c) Same but decoupled by MS with modes 1+2 ($h = 30$ mm). (d) Same but decoupled by MS with mode 4 ($h = 15$ mm).

IV. Experimental Verification

To study the decoupling regimes of the MS and to compare the proposed technique to the single-scatterer decoupling, we have measured S-parameters of two dipoles and the field patterns created by the active dipole in the presence of our MS with five wires and the single scatterer. The measurement process is described in Section II, while the experimental setup with the liquid phantom, two dipoles, and the five-wire MS is shown in Fig. 10.

The measured isolation $|S_{12}|^*$ at the frequencies of the low-order mode and high-order mode decoupling regimes of the MS (measured frequencies 280 and 293 MHz) depending on the height h are shown with marker curves in Fig. 6. As one can see, there is a good comparison between the achievable isolation levels in both regimes. The MS can decouple with the isolation of around −30 dB at $h = 30$ mm.

First, we discuss our side result. The experiment shows the presence of a low-order decoupling regime which confirms our expectations. Indeed, as follows from Fig. 9(d) the measured magnetic field pattern in the phantom looks similar to one in the case of the single scatterer [compare to Fig. 9(b)], but with not so sharp minimum of the field in the left part of the ROI. These measured patterns are in a good agreement with the simulation results presented in Fig. 7. Therefore, we confirmed that our MS can operate similarly in terms of decoupling and the field effect as a single scatterer. This is due to combination of modes 1 and 2. But in contrast to a single scatterer, it provides an additional and much more interesting

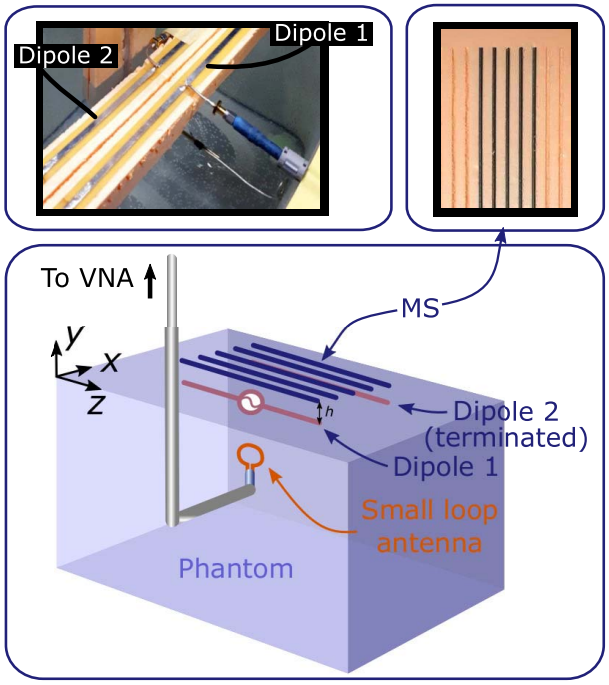

Fig. 10. Experimental setup for measurement of normalized magnetic field patterns created by active dipole in liquid phantom. Top-left inset: photograph of both active and matched dipoles are shown. Top-right inset: MS photograph is demonstrated.

narrow-band decoupling regime: based on resonant domination of mode 4.

Now let us discuss the main result, that is the narrow-band high-order decoupling regime due to mode 4. In this regime at the optimal height $h = 15$ mm, the isolation reaches -18 dB, while the measured pattern is shown in Fig. 9(c). It is seen that the shape of the field distribution in this case looks much closer to the field created by an individual active dipole as compared to the single scatterer decoupling and low-order decoupling regime of the same MS. Therefore, while reaching good isolation, mode 4 of the MS was experimentally shown to create weak destructive scattering. The optimal height for this mode differs from 10 mm predicted by the simulation, which can be explained to a very high sensitivity of isolation to the level of liquid in the phantom, which was difficult to control in the experiment within the accuracy of 2 mm. We note that there are some discrepancies between the simulated and measured H-field patterns such as the difference in the penetration depth of the field. These were caused mainly by the cable effect of probes, positioning of dipoles over the phantom and unstable conductivity of the latter in time. Nevertheless, the field interference minimum going from the top to bottom of the phantom is still clearly visible for the single scatterer. The same can be said about the low-order decoupling regime of the investigated MS. However, such a minimum is not observed in the reference case and with the MS operating in the high-order decoupling regime. Therefore, the experiment confirmed the existence of the desirable high-order decoupling regime with low radiation into a phantom.

V. Conclusion

In this article, a new resonant decoupling technique applicable for body MRI dipole array coils at 7 T was proposed and demonstrated. The technique uses a passive structure—an MS wire resonator—that needs to be placed above every pair of closely located dipoles. The MS is a very dense periodic grid of resonant wires and supports multiple eigenmodes in the 7-T MRI frequency range. For MSs of $N \geq 4$ wires, the fourth-order mode with antisymmetric distribution of currents can be excited by the active dipole and isolate it from the neighboring matched dipole with low parasitic scattering and field distortion in the ROI. The physical mechanism for this decoupling is based on the destructive interference of the primary field of the active dipole and the secondary field of the induced currents on MS wires. Indeed the primary and secondary fields in the case of the fourth mode at the decoupling frequency result in an almost zero total field along the matched dipole. In turn, the induced electromotive force acting on the matched dipole is suppressed.

Besides this high-order decoupling regime, for $N \geq 2$, there is a combination of the electric dipole (mode 1) with the electric quadrupole and the magnetic dipole (mode 2) that grants a very broad frequency band of decoupling, not achievable with a single wire scatterer having, however, almost the same field distortion.

For MS of $N = 5$ mode, 4 allows us to improve the isolation from -5 dB (no decoupling structure) down to -18 dB keeping the field pattern in the region of interest inside the body phantom similar to one of the active dipole alone. Though in free space, the corresponding decoupling band is very narrow (narrower than 0.1 MHz); in the presence of the phantom, this band increases up to 0.7 MHz and becomes compatible with the MRI application.

Our technique is dedicated for ultimately coupled dipoles antennas with the gap between them as small as $s = \lambda/30$. With an MS of four wires and more, located at the height from 1.5 to 2 wire periods, mode 4 is clearly observable in simulated and measured S-parameters of the dipoles and its decoupling frequency can be precisely tuned to the Larmor frequency by adjusting the length of the MS wires. The other known techniques of passive electromagnetic decoupling except for the single scatterer inserted in between the dipole antennas are not applicable in this case. Since our technique, while causing weak field distortion in the ROI, grants the same isolation level as the single-scatterer decoupling one and the operation bandwidth is sufficient for application in 7-T MRI, we believe in its high potential for ultrahigh field MRI.

Answering the three questions raised in Section I the obtained results allows to claim firstly that excitation of high-order modes in the wire MS grants the decoupling of the very dense dipole transceiver arrays. It was also numerically and experimentally shown that decoupling takes place also in the presence of the lossy homogeneous phantom—an averaged equivalent of the human body. The decoupling value wherein stays no lower than in the free space, while the decoupling bandwidth increases in the presence of a phantom. The main

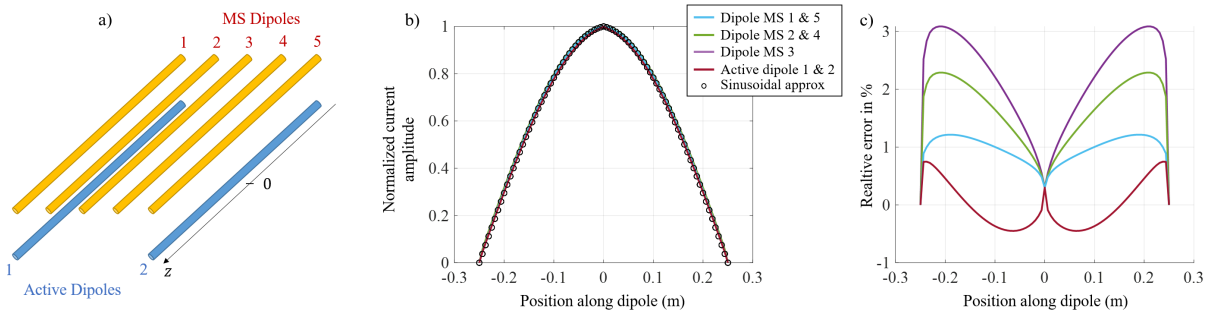

Fig. 11. (a) Sketch of the dipoles configuration. (b) Normalized current amplitude along the dipole obtained with Hallen's integral for each dipole. The open black circles show the sinusoidal distribution. (c) Relative error between Hallen's integral calculation and the sinusoidal distribution.

advantage of the decoupling by the wire MS high-order mode excitation compared to the single passive dipole decoupling is decreased scattered field resulting in reduction of active dipoles field distortion.

The proposed decoupling technique has been shown suitable for MRI dipoles. However, the narrow-band decoupling regime using the fourth mode was also observed in the absence of the phantom. Therefore, the technique can be also applied to isolate two closely spaced dipole antennas in free space. Its effect on the radiation pattern of the dipoles in comparison to a single-wire decoupling structure, as well as the general decoupling approach for dipoles with minimum distortion of far-fields, is a subject of future studies.

APPENDIX

A. Sinusoidal Current Distribution

The main argument in favor of the sinusoidal current assumption described in (1) is that the dipoles' length will be close to half a wavelength. To quantify the deviation to this equation, we computed the shape of the currents on each metallic element (two active dipoles + five passive MS dipoles), as shown in Fig. 11(a), using Hallen's integral equation for an array of dipoles. We set the voltage to be unity on each active dipole and zero for all passive MS dipoles (shortcut termination) with 80 current samples on each dipole. Fig. 11(b) and (c) shows the results of Hallen's integral equation. We observe a small deviation from the sinusoidal distribution approximation with a maximum relative error less than three percent that validates our original approximation.

B. Mutual Coupling Influence

As described in the manuscript, (2) expresses the mutual impedance between two dipoles without considering scattering from other elements. It has been reported that this method may present inaccuracies for dense arrays of active dipoles separated by less than $\lambda/4$ [33], [34]. Although there is no doubt that this observation is meaningful for applications such as array of numerous active antennas, it seems to be the case that our configuration with only two active antennas close to short circuited dipoles does not suffer from the same limitation. To support this claim, we compared the Z-matrix element obtained from our analytical method and results obtained from a commercial full-wave numerical solver

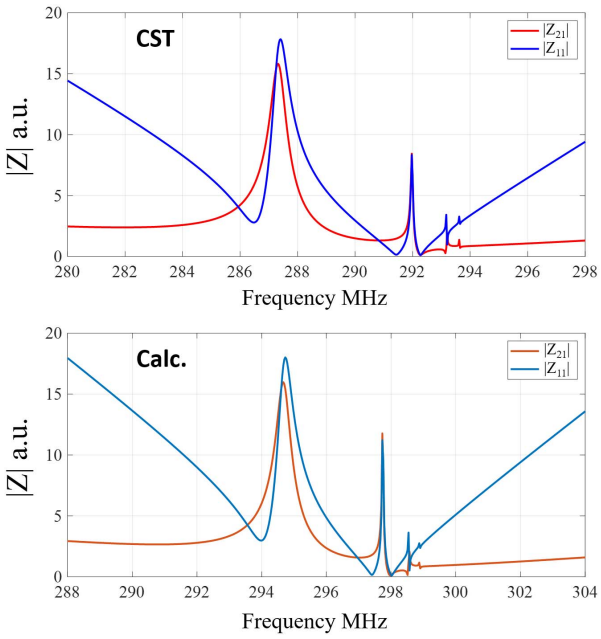

Fig. 12. Amplitude of Z-parameters obtained with CST (top) and our analytical calculation (bottom) in function of frequency. Due to the symmetry of the configuration the other two impedances (Z_{22} and Z_{12} are equal to those presented).

(CST Microwave studio 2019). In Fig. 12, we present the case of 8.5 mm spacing between the active dipoles and the MS.

We see from Fig. 12 that all the fine details originating from the interaction of the active dipoles and the MS resonances are perfectly captured and resolved by the analytical method. We observe a systematic discrepancy in terms of frequency dispersion and resonant frequency (2.5% shift) which is an acceptable consequence of our approximation regarding the $\lambda/30$ separation between the two active dipoles.

ACKNOWLEDGMENT

The authors are grateful to Dr. Alexander Raaijmakers of UMC Utrecht, Department of Radiotherapy, and Prof. Christophe Craeye, Université Catholique de Louvain, for useful discussions.

REFERENCES

[1] M. J. P. van Osch and A. G. Webb, "Safety of ultra-high field MRI: What are the specific risks?" *Current Radiol. Rep.*, vol. 2, no. 8, p. 61, Aug. 2014.

[2] J. T. Vaughan *et al.*, "Whole-body imaging at 7T: Preliminary results," *Magn. Reson. Med.*, vol. 61, no. 1, pp. 244–248, Jan. 2009.

[3] C. E. Hayes, W. A. Edelstein, J. F. Schenck, O. M. Mueller, and M. Eash, "An efficient, highly homogeneous radiofrequency coil for whole-body NMR imaging at 1.5 t," *J. Magn. Reson.*, vol. 63, no. 3, pp. 622–628, Jul. 1985.

[4] A. J. E. Raaijmakers *et al.*, "The fractionated dipole antenna: A new antenna for body imaging at 7 t esla," *Magn. Reson. Med.*, vol. 75, no. 3, pp. 1366–1374, Mar. 2016.

[5] G. C. Wiggins, B. Zhang, R. Lattanzi, G. Chen, and D. Sodickson, "The electric dipole array: An attempt to match the ideal current pattern for central SNR at 7 Tesla," in *Proc. 20th Annu. Meeting ISMRM*, Melbourne, VIC, Australia, vol. 541, 2012, p. 1.

[6] P. B. Roemer, W. A. Edelstein, C. E. Hayes, S. P. Souza, and O. M. Mueller, "The NMR phased array," *Magn. Reson. Med.*, vol. 16, no. 2, pp. 192–225, 1990.

[7] C. Thalhammer *et al.*, "Two-dimensional sixteen channel transmit/receive coil array for cardiac MRI at 7.0 T: Design, evaluation, and application," *J. Magn. Reson. Imag.*, vol. 36, no. 4, pp. 847–857, Oct. 2012.

[8] X. Yan, X. Zhang, B. Feng, C. Ma, L. Wei, and R. Xue, "7T transmit/receive arrays using ICE decoupling for human head MR imaging," *IEEE Trans. Med. Imag.*, vol. 33, no. 9, pp. 1781–1787, Sep. 2014.

[9] I. R. O. Connell, K. M. Gilbert, M. A. Abou-Khousa, and R. S. Menon, "Design of a parallel transmit head coil at 7T with magnetic wall distributed filters," *IEEE Trans. Med. Imag.*, vol. 34, no. 4, pp. 836–845, Apr. 2015.

[10] I. R. O. Connell, K. M. Gilbert, M. A. Abou-Khousa, and R. S. Menon, "MRI RF array decoupling method with magnetic wall distributed filters," *IEEE Trans. Med. Imag.*, vol. 34, no. 4, pp. 825–835, Apr. 2015.

[11] X. Yan, J. C. Gore, and W. A. Grissom, "Self-decoupled radiofrequency coils for magnetic resonance imaging," *Nature Commun.*, vol. 9, no. 1, pp. 1–12, Dec. 2018.

[12] A. A. Hurshkainen *et al.*, "Element decoupling of 7 t dipole body arrays by EBG metasurface structures: Experimental verification," *J. Magn. Reson.*, vol. 269, pp. 87–96, Aug. 2016.

[13] E. Georget *et al.*, "Stacked magnetic resonators for MRI RF coils decoupling," *J. Magn. Reson.*, vol. 275, pp. 11–18, Feb. 2017.

[14] D.-H. Kwon and D. H. Werner, "Restoration of antenna parameters in scattering environments using electromagnetic cloaking," *Appl. Phys. Lett.*, vol. 92, no. 11, Mar. 2008, Art. no. 113507.

[15] A. Monti, J. Soric, A. Alu, F. Bilotti, A. Toscano, and L. Vegni, "Overcoming mutual blockage between neighboring dipole antennas using a low-profile patterned metasurface," *IEEE Antennas Wireless Propag. Lett.*, vol. 11, pp. 1414–1417, 2012.

[16] G. Moreno *et al.*, "Wideband elliptical metasurface cloaks in printed antenna technology," *IEEE Trans. Antennas Propag.*, vol. 66, no. 7, pp. 3512–3525, Jul. 2018.

[17] B. K. Lau and J. B. Andersen, "Simple and efficient decoupling of compact arrays with parasitic scatterers," *IEEE Trans. Antennas Propag.*, vol. 60, no. 2, pp. 464–472, Feb. 2012.

[18] M. S. M. Mollaei, A. Hurshkainen, S. Kurdjumov, S. Glybovski, and C. Simovski, "Passive electromagnetic decoupling in an active metasurface of dipoles," *Photon. Nanostruct. Fundam. Appl.*, vol. 32, pp. 53–61, Dec. 2018.

[19] X. Yan and X. Zhang, "Decoupling and matching network for monopole antenna arrays in ultrahigh field MRI," *Quant. Imag. Med. Surgery*, vol. 5, no. 4, 2015.

[20] M. S. M. Mollaei, S. A. Kurdjumov, A. A. Hurshkainen, and C. R. Simovski, "Decoupling of two closely located dipoles by a single passive scatterer for ultra-high field MRI," *Prog. Electromagn. Res.*, vol. 164, pp. 155–166, 2019.

[21] A. P. Slobozhanyuk *et al.*, "Enhancement of magnetic resonance imaging with metasurfaces," *Adv. Mater.*, vol. 28, no. 9, pp. 1832–1838, 2016.

[22] A. Hurshkainen *et al.*, "A novel metamaterial-inspired RF-coil for preclinical dual-nuclei MRI," *Sci. Rep.*, vol. 8, no. 1, pp. 1–13, Dec. 2018.

[23] V. A. Ivanov, A. A. Hurshkainen, G. A. Solomakha, and M. A. Zubkov, "RF-coil with variable resonant frequency for multiheteronuclear ultra-high field MRI," *Photon. Nanostruct. Fundam. Appl.*, vol. 38, Feb. 2020, Art. no. 100747.

[24] S. B. Glybovski, S. A. Tretyakov, P. A. Belov, Y. S. Kivshar, and C. R. Simovski, "Metasurfaces: From microwaves to visible," *Phys. Rep.*, vol. 634, pp. 1–72, May 2016.

[25] S. J. Orfanidis, *Electromagnetic Waves and Antennas*. New Brunswick, NJ, USA: Rutgers Univ., 2002.

[26] M. Dubois *et al.*, "Kerker effect in ultrahigh-field magnetic resonance imaging," *Phys. Rev. X*, vol. 8, no. 3, Sep. 2018, Art. no. 031083.

[27] T. Otoshi, "On the scattering parameters of a reduced multiport," *IEEE Trans. Microw. Theory Techn.*, vol. MTT-17, no. 9, pp. 722–724, Sep. 1969.

[28] J. Rahola and J. Ollikainen, "Removing the effect of antenna matching in isolation analyses using the concept of electromagnetic isolation," in *Proc. Int. Workshop Antenna Technol., Small Antennas Novel Metamater.*, Mar. 2008, pp. 554–557.

[29] C. Jouvaud, R. Abdeddaim, B. Larrat, and J. de Rosny, "Volume coil based on hybridized resonators for magnetic resonance imaging," *Appl. Phys. Lett.*, vol. 108, no. 2, Jan. 2016, Art. no. 023503.

[30] R. E. Raab and O. L. de Lange, *Multipole Theory in Electromagnetism: Classical, Quantum, and Symmetry Aspects With Applications*. Oxford, U.K.: Oxford Science, 2005.

[31] G. Solomakha *et al.*, "The dual-mode dipole: A new array element for 7T body imaging with reduced SAR," *Magn. Reson. Med.*, vol. 81, no. 2, pp. 1459–1469, Feb. 2019.

[32] T. S. V. Gomez *et al.*, "Wireless coils based on resonant and nonresonant coupled-wire structure for small animal multinuclear imaging," *NMR Biomed.*, vol. 32, no. 5, May 2019, Art. no. e4079.

[33] H. T. Hui, "Improved compensation for the mutual coupling effect in a dipole array for direction finding," *IEEE Trans. Antennas Propag.*, vol. 51, no. 9, pp. 2498–2503, Sep. 2003.

[34] C. Craeye and D. González-Ovejero, "A review on array mutual coupling analysis," *Radio Sci.*, vol. 46, no. 2, pp. 1–25, 2011.